ACS APPLIED MATERIALS & INTERFACES

Research Article

Cite This: ACS Appl. Mater. Interfaces 2019, 11, 6541−6549

www.acsami.org

Elastomer-Free, Stretchable, and Conformable Silver Nanowire Conductors Enabled by Three-Dimensional Buckled Microstructures

Chuanxin Weng,[†,‡] Zhaohe Dai,[§] Guorui Wang,[†] Luqi Liu,[*,†] and Zhong Zhang[*,†]

[†]CAS Key Laboratory of Nanosystem and Hierarchical Fabrication and CAS Center for Excellence in Nanoscience, National Center for Nanoscience and Technology, Beijing 100190, China

[‡]University of Chinese Academy of Sciences, Beijing 100049, China

[§]Center for Mechanics of Solids, Structures and Materials, Department of Aerospace Engineering and Engineering Mechanics, The University of Texas at Austin, Austin, Texas 78712, United States

Supporting Information

ABSTRACT: Many three-dimensional (3D) nanomaterial-based assemblies need incorporation with elastomers to attain stretchability—that also compromises their pristine advantages for functional applications. Here, we show the design of elastomer-free, highly deformable silver nanowire (AgNW) conductors through dip-coating AgNWs on a 3D polymeric scaffold and following a simple triaxial compression approach. The resulting 3D AgNW conductors exhibit good stability of resistance under multimodal deformation, such as stretching, compressing, and bending as well as comparable conductivity with those elastomer-based ones. Moreover, the buckled structures endow our 3D conductors with novel negative Poisson's ratio behavior, which can offer good comfortability to curvilinear surfaces. The combination of mechanical properties, conductive performance, and unique deformation characteristics can satisfy multiscale conformal mechanics with a soft, curvilinear human body.

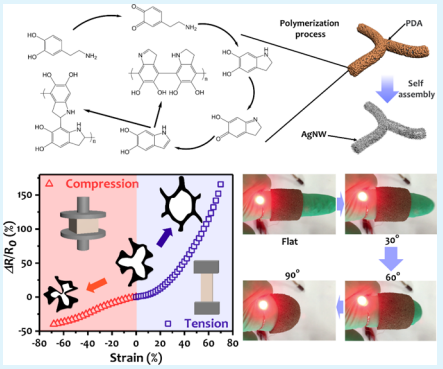

KEYWORDS: *stretchable conductors, silver nanowire, buckling, negative Poisson's ratio, conformability*

1. INTRODUCTION

Stretchable electronic materials enable classes of applications, such as flexible sensors[1−4] and actuators,[5,6] electronic textiles,[7−9] deformable displays,[10,11] and artificial skins,[12−15] that cannot be achieved using conventional, wafer-based technologies. Developing materials that can offer the conductive properties of established inorganic materials but also can endure multimodal, large-strain, and repeated deformations without changes in their characteristics is of crucial importance in this field. Besides structurally upgrading the stretchability of conventional inorganic and metallic materials, bottom-up assembly of nanomaterials—that have remarkable electrical properties and can intrinsically survive large deformations—represents an alternative and particularly promising routine. Advances in the context can be roughly categorized by the bulk configurations of these assemblies: one-dimensional (1D) yarns and fibers,[16−19] two-dimensional (2D) conductive sheets, mats, and films,[20,21] and three-dimensional (3D) arrays, sponges, and foams.[22−25] The building blocks used include nanocarbon materials, such as carbon nanotubes (CNTs) and graphene,[16,26−28] and nanometal materials, such as silver, copper, and gold nanoparticles or nanowires.[24,29−31]

A major challenge limiting the application of nanomaterials in flexible electronics is the loss of stretchability and mechanical robustness after assembling them to bulk materials. Such fact has been believed to be a result of the relatively weak interfacial interaction between individual nanomaterials.[32] One way to overcome this challenge is to introduce buckled, curved microstructures into these assemblies such that the bulk deformation mostly comes from the stretchable microstructures, instead of the weak interfaces nor relatively stiff nanomaterials themselves. Recent developments have led to a combination of bottom-up and top-down manufacturing strategies to achieve nanomaterial-based assemblies with stretchable microstructures. Examples include twisting the CNT yarn to form a springlike configuration,[33] designing an in-plane serpentine shape with kirigami techniques,[34,35] exploiting the stretching/release/buckling method to achieve out-of-plane waviness for CNT ribbons on an elastomer,[36] and many more. However, unlike those 1D and 2D examples, 3D assemblies show more intriguing structural hierarchy, yet the introduction of stretchability-favored bucklings into them in a controlled manner has been extremely challenging. Consequently, these 3D assemblies, such as graphene, CNT, and nanowire foams/sponges, were incorporated with elastomers to attain stretchability. This treatment compromises many of the advantages of the pristine assemblies, such as low density,

Received: November 12, 2018
Accepted: January 16, 2019
Published: January 16, 2019

DOI: 10.1021/acsami.8b19890
ACS Appl. Mater. Interfaces 2019, 11, 6541−6549

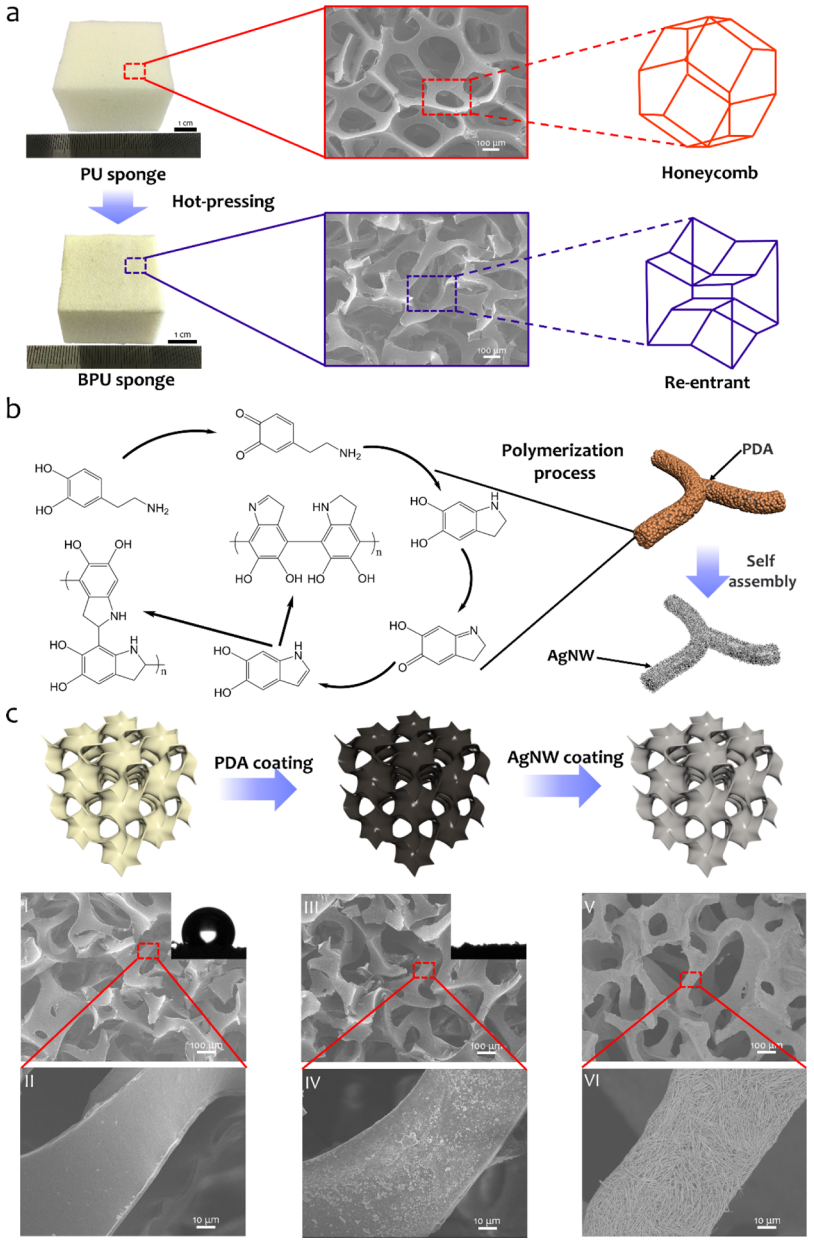

Figure 1. Preparation and characterization of the AgNW-coated BPU sponge. (a) Comparison between PU and BPU sponges. (b) Polymerization process of PDA and a diagrammatic representation for self-assembly of the AgNW. (c) Schematic illustration of the manufacture of the AgNW-coated BPU sponge. (I,II) SEM pictures of the BPU sponge at low and high magnification, respectively. (III,IV) SEM pictures of the PDA-coated BPU sponge at low and high magnification, respectively. (V,VI) SEM pictures of the AgNW-coated BPU sponge at low and high magnification, respectively.

permeability, and high aspect specific surface area, features that would extend their functional uses. Also, a hard nanomaterial–soft elastomer mismatch makes interfacial failure nontrivial, challenging their long-term durability as stretchable electronic elements.

Here, we describe the design of 3D elastomer-free, stretchable, compressible, and bendable silver nanowire (AgNW) conductors via a simple triaxial buckling approach. We chose commercially available polyurethane (PU) sponges as templates because of their available open-cell, high deformability, and large specific surface area, that is, suitable for coating on kinds of nanomaterials and introduced with a buckled structure by triaxial thermal compression. Before dip-coating the AgNW on the buckled template, the sponge scaffold was modified with polydopamine (PDA) layers to improve the adhesion between nanowires and the scaffold. The resulted conductors possess remarkable deformability, conductivity, and stability. Also, the stretchable conductors, showing interesting negative Poisson's ratio, can provide good comfortability to curvilinear surfaces, which are common in the human body.

2. RESULTS AND DISCUSSION

2.1. Preparation and Characterization of Buckled Sponges. The buckled sponges were prepared based on the previous study.[26,37,38] Figure 1a shows the process of fabrication and the comparison between PU and buckled PU (BPU) sponges, where the buckled structure was introduced to

DOI: 10.1021/acsami.8b19890
ACS Appl. Mater. Interfaces 2019, 11, 6541−6549

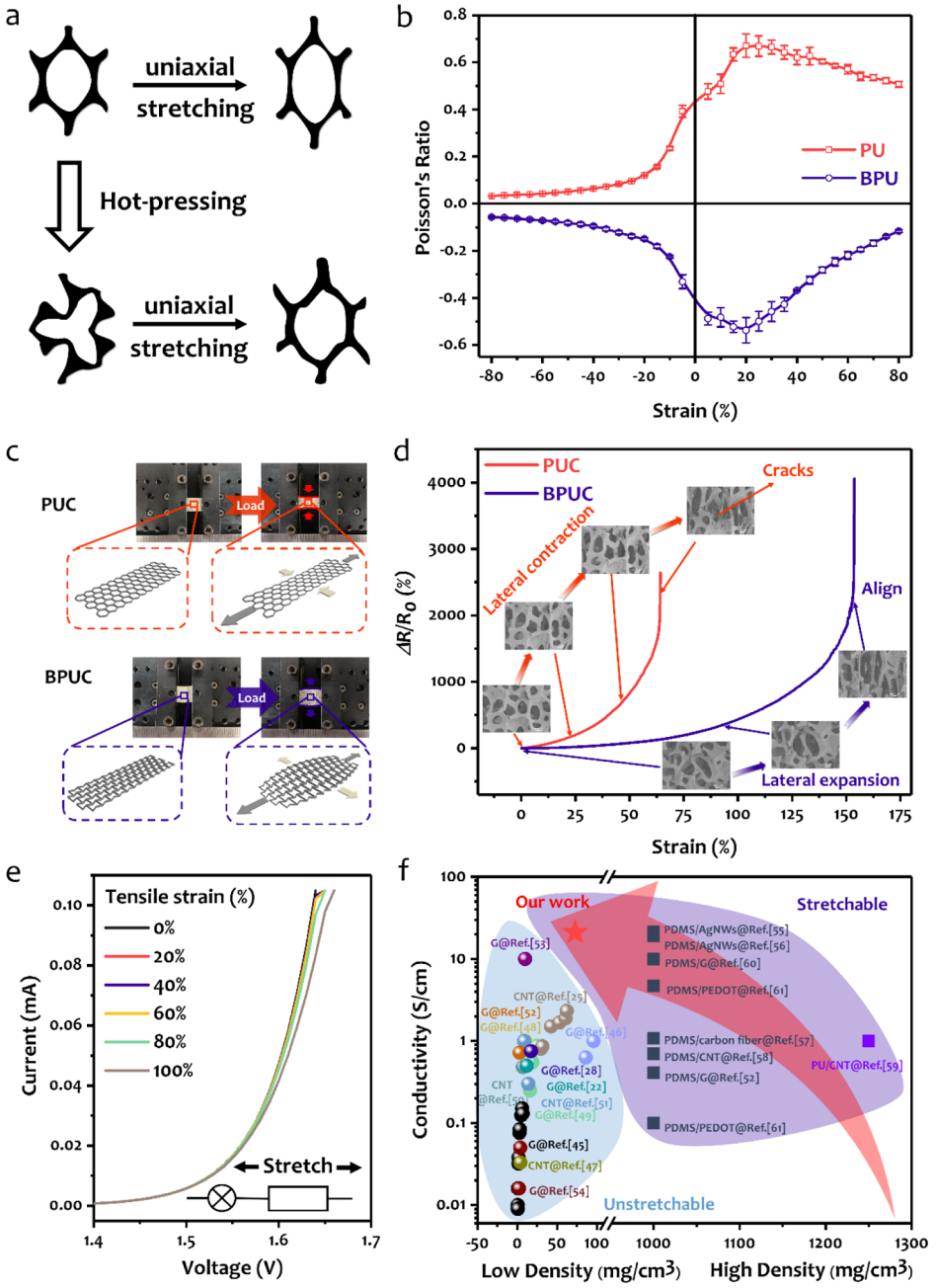

Figure 2. (a) Schematic of the structure conversion under uniaxial stretching. (b) Poisson's ratio of PU and BPU sponges under tensile and compressive strain. (c) Photograph of PUC and BPUC under stretching. Representative lateral contraction for PUC and lateral expansion for BPUC under tension with different structures. (d) Variation of relative resistance change concerning tensile strain for both conventional PUC and BPUC. The in situ tension with SEM shows the conversion of the internal structure of PUC and BPUC. (e) Current−voltage measurement of LED lamps connected by stretchable BPUC at various tensile strains. (f) Comparison of the conductivity properties of BPUC and other materials as a function of density. (G: graphene foam).

commercial PU sponges with a triaxial compression. A comparison of internal structures is further made between the conventional pristine PU and the BPU sponges. As shown in Figure 1a, the pristine PU sponge presents a honeycomb-like structure,[38] while the BPU sponge presents a buckled structure with a hot-pressing treatment, which can be regarded as a re-entrant structure, as evidenced by the scanning electron microscopy (SEM) images (Figure 1a).

Subsequently, in order to facilitate comparison, both of the commercial PU sponge and the BPU sponge were dealt with the following steps, as shown in the schematics in Figure 1b. The first step is to modify an adhesion layer on the surface of the sponge. As known, the PDA coating is an effective method to modify various surfaces because of its abundant catechol and amine groups.[39−41] As shown in Figure 1b, dopamine will undergo self-polymerization to produce an adherent PDA coating on the surface of the sponge at a weak alkaline pH. A transition of color from white to black is clearly observed for BPU after coating the PDA layer. Meanwhile, the surface of the BPU sponge shows the transition from the hydrophobic characteristic as shown in Figure 1c(I) to the hydrophilic characteristic as demonstrated by contact angle measurements

DOI: 10.1021/acsami.8b19890
ACS Appl. Mater. Interfaces 2019, 11, 6541−6549

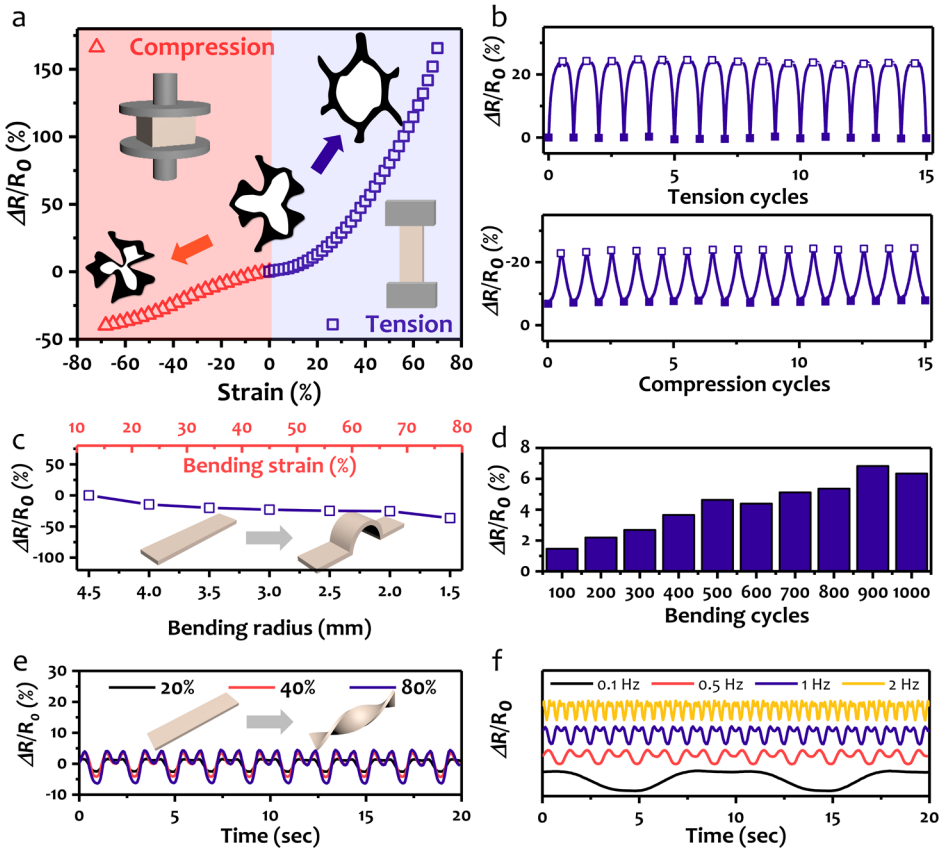

Figure 3. Conductive performance under multimodal deformation of BPUC. (a) Relative resistance change under strain (the negative and positive strains represent compressive and tensile strains, respectively) the inset is the process of structure evolution under the tensile strain and compressive strain. (b) Relative change in resistance within 15 cycles under tensile strain (0−50%) and compressive strain (−10 to −50%). (c) Relative change in resistance under bending deformation. The inset is the schematic of the bending mode. (d) Relative resistance change for BPUC under 1000 bending cycles (bending radius: 3 mm). (e) Resistance change for BPUC under different twisting strains. (f) Resistance change for BPUC under various frequencies at 40% strain.

in the inset of Figure 1c(III). To endow the electrical performance of the BPU sponge, AgNWs were coated through multiple dip-coating cycles in the AgNW suspension (with a concentration of 5 mg/mL and the aspect ratio is close to 1000 for the AgNW). Note that the four-cycle treatment is optimized to achieve the uniform AgNW coating and hence a high conductivity around 20 S/cm and a comparatively low density of 73 mg/cm^3 (Figures 1c(V,VI), S4, and S5). The final content of the AgNW was ∼18 wt % as determined by thermogravimetric analysis (TGA, Figure S5). In comparison with PDA-assisted AgNW/BPU shown in Figure 1c(V,VI), only few AgNW could be observed on the surface of PU without the presence of the PDA layer (Figure S6), indicating that the presence of the PDA layer is vital for enhancing the adhesion between AgNW and PU surfaces. We attributed it to the hydrogen bonding-driven self-assembly between lone pair electrons of catechol and amine groups on the surface of PDA and the carbonyl groups of the polyvinyl pyrrolidone (PVP)-modified AgNW.[42,43] Additionally, this simple approach favors large-scale fabrication and the size of conductors can reach as large as 100 cm^2 (Figure S7).

2.2. Poisson's Ratio and Conductive Performance. Generally, Poisson's ratio provides a universal way to contrast the structural performance of materials when strained elastically. In particular, negative Poisson's ratio (auxetic behavior), that is, the anomalous property of becoming wider rather than thinner when stretched, has been demonstrated to trigger some remarkable properties for practical applications.[44] On the basis of the SEM images of the internal structure in Figure 1a, we can assume that the internal porous structures of PU and BPU feature the regular hexagonal and indented hexagonal shape, respectively. In addition, the structural evolution under uniaxial stretching for different shapes is shown in Figure 2a. In addition, as shown in Figure 2b, Poisson's ratio of PU and BPU sponges is totally different, which is positive for PU and negative for BPU regardless of deformation modes. More interestingly, Poisson's ratio for BPU almost tends to be around −0.5 within 30% tensile strain and the smallest of −0.54 at 20% tensile strain. Figure 2c shows the comparison between the PU conductors (PUC) and BPU conductors (BPUC) under uniaxial stretching, where distinct deformation characteristics are obviously visible.

To further investigate the effects of the buckled structure on the conductive performance, we have studied the relative resistance change ($\Delta R/R_0$) in the axial direction against the applied strain for both PUC and BPUC (Figure 2d). As expected, PUC (red curve) display a dramatic enhancement in $\Delta R/R_0$ as the tensile strain increases and eventually fracture at the strain of 65% with a 26 times increase in resistance. By comparison, the BPUC (blue curve) show a significantly better conductive performance over a broad range of strain (the conductivity is shown in the Figure S9), including higher stability below the strain of 75% and greater deformability

DOI: 10.1021/acsami.8b19890
ACS Appl. Mater. Interfaces 2019, 11, 6541−6549

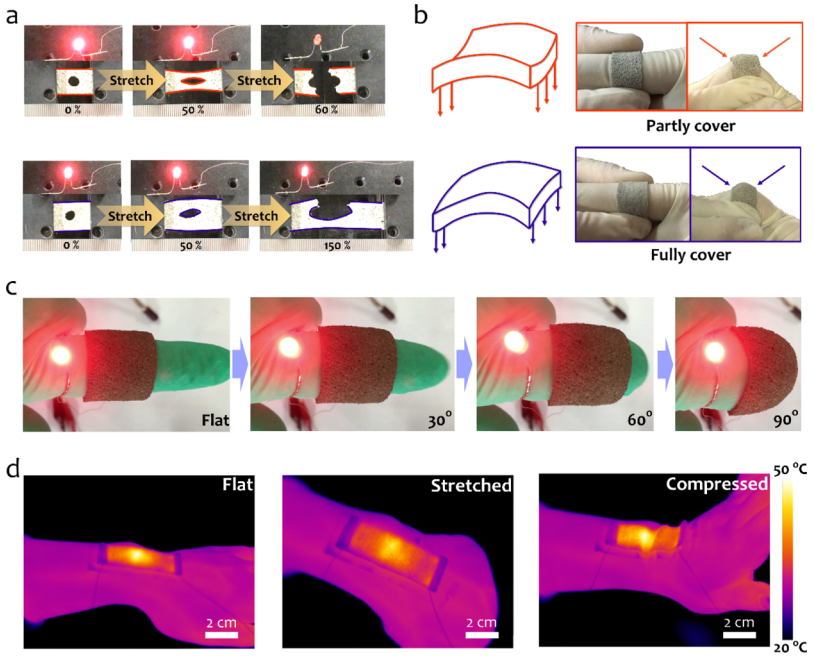

Figure 4. Representative properties of BPUC. (a) Digtal images of crack resisting under tensile strain for both PUC and BPUC. (b) Left: Schematic illustration of different curvatures for PUC and BPUC. Right: Photographs of PUC and BPUC attached on the joint of the finger. (c) Photographs of LED lamp-integrated BPUC attached on the finger with different bending angles, from 0° to 90°. (d) Infrared images of BPUC attached on a wrist under movement.

beyond that. To study the effect of the internal structure on the conductive properties, a homemade in situ tensile machine was employed to monitor the evolution process of the internal structure under different tensile stains. As shown in insets of Figure 2d, when BPUC are under tension, their re-entrant structures enable buckled structure-releasing deformations (in both the stretching direction and the transverse direction), instead of separation of conductive nanomaterials, so as to guarantee the stability of resistance even under large tensile strains. On the contrary, for the PUC with positive Poisson's ratio, the deformation in the transverse direction is always opposite to the stretching direction. Thus, there would be many cracks when stretching the PUC as observed from the SEM views, which leads to rapidly increasing resistance.

To confirm the superior conductive stability of BPUC, we designed a complete circuit, where the conductive sponges served as conductors connected with a red light-emitting diode (LED), clamped by our homemade tensile machine. As shown in Figure S10, with the increase in tensile strain, distinct LED emission intensities are observed. For the PUC, the LED emission intensity merely maintains below the tensile strain of 50%, while higher strains would cause ultimate fracture that decreases the emission intensity. In contrast, for the BPUC, the LED emission intensity remains almost unvaried during the whole stretching deformation process until the strain up to 100%. As a proof-of-concept of the application of the BPUC, we demonstrated the fabrication of the stretchable LED circuit to light up an LED lamp at different tensile strains (Figure 2e) and found an excellent stability of $I-V$ characteristics curves within the range from 0 to 100%.

Furthermore, our stretchable conductors also exhibit advantages in both conductive performance and material density (Figure 2f) as compared with other recently reported 3D spongelike materials, including carbon foams/aerogels[22,25,28,45−54] (the density is within 100 mg/cm^3) and elastomeric substrate-based conductors[52,55−61] [such as polydimethylsiloxane (PDMS), PU, Ecoflex, and so on, and the density based on the substrate is at least 1000 mg/cm^3]. Specially, the density of our conductors is as low as 73 mg/cm^3, which is commensurable to carbon materials and far below elastomeric substrate-based conductors. The conductivity can be maintained as high as 14 S/cm with excellent stability within tensile strain of up to 50%. Not only with the stretchability, our stretchable conductors also possess the same compressibility as carbon foams with stable conductivity, in striking contrast with the elastomeric substrate-based conductors that can only suffer compressive strain of 10% reversibly.[50]

2.3. Conductive Capability under Multimodal Deformation. The cycling stability of the stretchable conductors is one of the most important characters, as it determines the reusability of stretchable conductors or even wearable electronics. Herein, to testify the cycling stability of the BPUC, the dynamic thermomechanical analysis (DMA) machine was used to apply tensile cycle deformations, while the resistance was measured by Keithley 4200. Figure 3a shows $\Delta R/R_0$ as a function of strain (the negative and positive strains represent compressive and tensile strains, respectively), and the stretching/releasing and compressing/releasing cycles are presented in Figure 3b. During stretching/releasing cycles, we find that $\Delta R/R_0$ is only ∼25% at a strain of 50%, corresponding to the resistance of about 1.16 Ω, and this value further drops down to ∼23% during compressing/releasing cycles for the BPUC. In addition, the response of $\Delta R/R_0$ under different tensile and compressive strains has also been shown in Figure S12. In comparison with the recent report, conductors of the Au−Ni@graphene-coated PU sponge based on elastomeric PDMS represented almost 100% of $\Delta R/R_0$ at a tensile strain of 30%;[62] another case such as graphene honeycomb sandwich integrated with PDMS showed

DOI: 10.1021/acsami.8b19890
ACS Appl. Mater. Interfaces 2019, 11, 6541−6549

60% fluctuation for 60% tensile strain;[52] the excellent cycling stability of the BPUC declares the competence of being a stretchable conductor.

In addition to the tension mode, other deformation modes including bending and twisting have been executed to evaluate the cycling stability of BPUC. As depicted in Figure 3c, with decreasing bending radius, the as-resulted increasing bending strain tends to slightly reduce the resistance of the BPUC. Moreover, the performance of the cycling stability under the bending mode is excellent as the $\Delta R/R_0$ is less than 10% after 1000 cycles at a given bending radius of ∼3 mm, as shown in Figure 3d. However, keep increasing the bending cycles, $\Delta R/R_0$ increased slightly, and the SEM image also shows that there are some cracks but the conductive path remains intact, as shown in Figure S13. Similar stability was also observed for the twisting mode as $\Delta R/R_0$ is within 7% under the cyclic twisting strains at different levels, even under a dynamic conductive environment as demonstrated in Figure 3e,f (frequencies ranging from 0.1 to 2 Hz with a twisting strain of 40%).

2.4. Potential Application of BPUC. Despite of the excellent conductivity, stretchability, and stability under multimodal deformation, the BPUC also possess other special properties that are well suited for wearable electronics. As shown in Figure 4a, circular holes are present in the middle of both the PUC and BPUC and LED lights are integrated to examine the mechanical response of sponges to structural defects. Initially, both the PUC and BPUC can maintain the structural integrity so that the LED lights always kept bright. However, with the continuous increase of the tensile strain beyond 50%, the circular hole in PUC tends to be a longer and narrower slit which facilitates the fast fracture of the conductors. In contrast, because of the re-entrant structures and auxetic deformation behaviors of BPUC, the circular hole is likely to form an ellipse shape during tension, so that the relatively uniform strain distribution could effectively retard the propagation of cracks and enable a considerably high stretchability (a fracture strain of 150%) even with a structural defect.

Additionally, combined with such great stretchability, negative Poisson's ratio makes our stretchable conductors highly accommodated to body movements, such as bending of the finger, wrist, and elbow, thus satisfying the demands for wearable electronics. As illustrated in Figure 4b, compared with the PUC with positive Poisson's ratio that features the anticlastic curvature under bending, the BPUC with negative Poisson's ratio tend to exhibit synclastic characters which improves its fitness for the irregular and movable surface. Such distinction can be clearly seen in the photos in the right side as an example, demonstrating higher conformability and comfortability of BPUC when tied to the finger and subjected to bending. Furthermore, employing the same method as discussed above, the stability of conductive performance is also verified under bending deformation without loss of its conformability on the finger joint, as shown in Figure 4c.

Owing to the excellent conductivity under multimodal deformation, our materials are also suitable for the stretchable heaters.[63−65] The curves of temperature against time are plotted at different direct voltages, and eventually, the temperature tends to stabilize at a constant value (Figure S15). Herein, the electrical heater is integrated with a direct current power and tied on the wrist, and Figure 4d shows a series of infrared camera images when the wrist moved downward and upward during joule heating at an applied voltage of ∼1.2 V. This proves the remarkable stability of the heater under deformation and its potential as the stretchable heaters. In attention, compared with other heaters,[63−65] our designed stretchable heaters possess lower driving voltage for heating, and the porous and buckled structure endows comfortability unlike the elastomeric polymer, for example, gas permeability and adaptability for complex shapes.

3. CONCLUSIONS

In conclusion, we have successfully developed 3D multimodal deformation electrically conductive conductors by the fabrication of a thin layer of the AgNW on chemically modified, 3D-interconnected, and macroscopically continuous BPU sponges with negative Poisson's ratio by introducing the buckled structure through the 3D hot-pressing process. Furthermore, this method has several remarkable advantages. First, the sponges are a highly interconnected porous structure, which provides a template for the AgNW to build a 3D conductive network. Second, the modified surface increases the adhesion and interfacial strength. Third, the introduction of the buckled structure not only enhances the stretchability but also guarantees the conductive stability as stretchable conductors based on the buckled structure-releasing effect. Finally, the fabrication process is air-compatible and solution-processed, which is suitable for large-scale production and applications.

Furthermore, compared with the general PUC, negative Poisson's ratio behavior of BPUC provides a unique advantage, that is, particularly beneficial to the stretchable conductors and other devices. Also, due to negative Poisson's ratio, the BPUC possess some special characters. For example, the crack resistance makes the BPUC maintain stable performance even with severe damage. Another is the unique shape-conforming capability because of the synclastic curvature property when bending to form doubly curved or domed shapes, which is not possible in any other positive Poisson's ratio materials. Considering the complex human body contours containing various double curvature surfaces, these conductors can fit the curvature surface of body's joint perfectly and satisfy the dynamic moving process. We also successfully demonstrated the potential application of the BPUC, and the excellent conductive performance was presented under different deformations. Although it is only a proof-of-concept demonstration, we envision that the 3D stretchable and compressible and electrically conductive BPUC should have many applications in flexible and wearable electronics, electronic skins, actuators, and so forth.

4. EXPERIMENTAL SECTION

4.1. Preparation of BPU Sponges. The commercially available open-cell PU sponges were first cut into 45 × 45 × 30 mm^3 cuboids and then cleaned by ethanol and deionized water, followed by drying at 60 °C for 4 h. One of these sponges was then inserted into a steel mold (inside dimensions 30 × 30 × 20 mm^3) and compressed triaxially with compressive strain of 33.3% in all three orthogonal directions. The steel mold was then pressed under the hot-pressing machine for 1 h at softening temperature (150 °C). After cooling to room temperature, the sponge was removed from the mold.

4.2. Preparation of PDA-Modified BPU Sponges. The BPU sponge was cleaned by ethanol several times and dried at 40 °C. The cleaned BPU sponge was cut into small pieces with a size of 30 × 5 × 2 mm^3. Tris(hydroxymethyl) aminomethane (0.242 g) was dissolved in 200 mL of distilled water, and the pH was maintained at 8−9 with HCl. Then, 0.2 g of dopamine hydrochloride was added and

DOI: 10.1021/acsami.8b19890
ACS Appl. Mater. Interfaces 2019, 11, 6541−6549

dissolved. All sponge pieces were dipped into the solution for 12 h and then dried at 40 °C for 2 h.

4.3. Preparation of the AgNW. The AgNW for the preparation of stretchable conductors was synthesized using a one-step polyol method.[66,67] PVP (6 g, MW = 300 000) was added to 150 mL of ethylene glycol (EG) and wholly dissolved using magnetic stirring at room temperature. Afterward, 5 g of silver nitrate ($AgNO_3$) was added to the PVP solution. After complete dissolution, 20 g of a $CuCl_2$ salt solution (50 mM in EG) was dumped into the mixture and stirred for 3 min at room temperature. The mixture was then heated at 130 °C to grow the AgNW for 1 h until the reaction was complete. Finally, acetone and ethanol were used to wash the precipitate.

4.4. Preparation of BPUC. The modified BPU sponge was immersed in the AgNW dispersion for 30 min and then blew away the excess AgNW by nitrogen. The dip-coating process was repeated until the surface of BPU was fully coated, and the resulted AgNW-coated sponge was dried overnight.

4.5. Characterization. The morphologies the samples were examined by a scanning electron microscope (JEOL JSM-7500F). The 3D internal structure of BPUC was tested by ZEISS Xradia 510 versa. The in situ observation was executed by our homemade in situ tension machine. The content of the AgNW was measured on TGA Q500 (TA) by heating from room temperature to 1000 °C in nitrogen at 10 °C min^{-1}. The temperature of BPUC at different voltages was recorded by a simple thermocouple, and the infrared images were recorded on Fluke Thermal Imager TiX 560.

4.6. Conductive Performance Evaluation. The electrical resistance of the conductive BPUC under multimodal deformation was tested by a four-wire probe method with a Keithley 4200 sourcemeter. The stretching (the sample size is 30 × 5 × 2 mm^3) and compression (the sample size is 10 × 10 × 8 mm^3) tests were performed on DMA Q800 (TA), the bending (the sample size is 30 × 5 × 2 mm^3) tests were executed by homemade tension clamp, and the twisting (the sample size is 30 × 5 × 2 mm^3) tests were carried out on a HAAKE MARS II rheometer.

■ ASSOCIATED CONTENT

Supporting Information

The Supporting Information is available free of charge on the ACS Publications website at DOI: 10.1021/acsami.8b19890.

Fabrication process for BPU, size of pore and backbone for PU and BPU sponges, diameter and length for AgNW and AgNW content and conductivity of BPUC with different coating cycles, morphologies for AgNW-coated PU with and without the PDA layer, relative change in resistance under different strains (tensile and compressive), temperature at different dc voltages for BPUC, morphologies for BPUC after tensile and bending cycles, and 3D structure for BPUC (PDF)

■ AUTHOR INFORMATION

Corresponding Authors

*E-mail: liulq@nanoctr.cn (L.L.).
*E-mail: zhong.zhang@nanoctr.cn (Z.Z.).

ORCID

Zhaohe Dai: 0000-0002-5205-089X
Luqi Liu: 0000-0002-5752-1638
Zhong Zhang: 0000-0002-9102-1311

Notes

The authors declare no competing financial interest.

■ ACKNOWLEDGMENTS

This project was supported by the National Natural Science Foundation of China (grant no. 21474023) and National Key Basic Research Program of China (grant no. 2013CB934203).

■ REFERENCES

(1) Kaltenbrunner, M.; Sekitani, T.; Reeder, J.; Yokota, T.; Kuribara, K.; Tokuhara, T.; Drack, M.; Schwödiauer, R.; Graz, I.; Bauer-Gogonea, S.; Bauer, S.; Someya, T. An Ultra-Lightweight Design for Imperceptible Plastic Electronics. *Nature* **2013**, *499*, 458−463.

(2) Drack, M.; Graz, I.; Sekitani, T.; Someya, T.; Kaltenbrunner, M.; Bauer, S. An Imperceptible Plastic Electronic Wrap. *Adv. Mater.* **2014**, *27*, 34−40.

(3) Kim, D.-H.; Lu, N.; Ma, R.; Kim, Y.-S.; Kim, R.-H.; Wang, S.; Wu, J.; Won, S. M.; Tao, H.; Islam, A.; Yu, K. J.; Kim, T.-i.; Chowdhury, R.; Ying, M.; Xu, L.; Li, M.; Chung, H.-J.; Keum, H.; McCormick, M.; Liu, P.; Zhang, Y.-W.; Omenetto, F. G.; Huang, Y.; Coleman, T.; Rogers, J. A. Epidermal Electronics. *Science* **2011**, *333*, 838−843.

(4) Lipomi, D. J.; Vosgueritchian, M.; Tee, B. C.-K.; Hellstrom, S. L.; Lee, J. A.; Fox, C. H.; Bao, Z. Skin-like Pressure and Strain Sensors Based on Transparent Elastic Films of Carbon Nanotubes. *Nat. Nanotechnol.* **2011**, *6*, 788−792.

(5) Tao, H.; Hwang, S.-W.; Marelli, B.; An, B.; Moreau, J. E.; Yang, M.; Brenckle, M. A.; Kim, S.; Kaplan, D. L.; Rogers, J. A.; Omenetto, F. G. Silk-based Resorbable Electronic Devices for Remotely Controlled Therapy and in Vivo Infection Abatement. *Proc. Natl. Acad. Sci. U.S.A.* **2014**, *111*, 17385−17389.

(6) Farra, R.; Sheppard, N. F.; McCabe, L.; Neer, R. M.; Anderson, J. M.; Santini, J. T.; Cima, M. J.; Langer, R. First-in-Human Testing of a Wirelessly Controlled Drug Delivery Microchip. *Sci. Transl. Med.* **2012**, *4*, 122ra21.

(7) Service, R. F. TECHNOLOGY: Electronic Textiles Charge Ahead. *Science* **2003**, *301*, 909−911.

(8) Pang, C.; Lee, C.; Suh, K.-Y. Recent Advances in Flexible Sensors for Wearable and Implantable Devices. *J. Appl. Polym. Sci.* **2013**, *130*, 1429−1441.

(9) Hu, L.; Pasta, M.; La Mantia, F.; Cui, L.; Jeong, S.; Deshazer, H. D.; Choi, J. W.; Han, S. M.; Cui, Y. Stretchable, Porous, and Conductive Energy Textiles. *Nano Lett.* **2010**, *10*, 708−714.

(10) Sekitani, T.; Nakajima, H.; Maeda, H.; Fukushima, T.; Aida, T.; Hata, K.; Someya, T. Stretchable Active-Matrix Organic Light-Emitting Diode Display Using Printable Elastic Conductors. *Nat. Mater.* **2009**, *8*, 494−499.

(11) Kim, S.; Kwon, H.-J.; Lee, S.; Shim, H.; Chun, Y.; Choi, W.; Kwack, J.; Han, D.; Song, M.; Kim, S.; Mohammadi, S.; Kee, I.; Lee, S. Y. Low-Power Flexible Organic Light-Emitting Diode Display Device. *Adv. Mater.* **2011**, *23*, 3511−3516.

(12) Wu, X.; Ma, Y.; Zhang, G.; Chu, Y.; Du, J.; Zhang, Y.; Li, Z.; Duan, Y.; Fan, Z.; Huang, J. Thermally Stable, Biocompatible, and Flexible Organic Field-Effect Transistors and Their Application in Temperature Sensing Arrays for Artificial Skin. *Adv. Funct. Mater.* **2015**, *25*, 2138−2146.

(13) Lee, J.-H.; Lee, K. Y.; Gupta, M. K.; Kim, T. Y.; Lee, D.-Y.; Oh, J.; Ryu, C.; Yoo, W. J.; Kang, C.-Y.; Yoon, S.-J.; Yoo, J.-B.; Kim, S.-W. Highly Stretchable Piezoelectric-Pyroelectric Hybrid Nanogenerator. *Adv. Mater.* **2013**, *26*, 765−769.

(14) Yeo, W.-H.; Kim, Y.-S.; Lee, J.; Ameen, A.; Shi, L.; Li, M.; Wang, S.; Ma, R.; Jin, S. H.; Kang, Z.; Huang, Y.; Rogers, J. A. Multifunctional Epidermal Electronics Printed Directly Onto the Skin. *Adv. Mater.* **2013**, *25*, 2773−2778.

(15) Hammock, M. L.; Chortos, A.; Tee, B. C.-K.; Tok, J. B.-H.; Bao, Z. 25th anniversary article: The Evolution of Electronic Skin (e-skin): a Brief History, Design Considerations, and Recent Progress. *Adv. Mater.* **2013**, *25*, 5997−6038.

(16) Xu, Z.; Liu, Y.; Zhao, X.; Peng, L.; Sun, H.; Xu, Y.; Ren, X.; Jin, C.; Xu, P.; Wang, M.; Gao, C. Ultrastiff and Strong Graphene Fibers via Full-Scale Synergetic Defect Engineering. *Adv. Mater.* **2016**, *28*, 6449−6456.

(17) Xu, Z.; Gao, C. Graphene Chiral Liquid Crystals and Macroscopic Assembled Fibres. *Nat. Commun.* **2011**, *2*, 571.

(18) Kou, L.; Huang, T.; Zheng, B.; Han, Y.; Zhao, X.; Gopalsamy, K.; Sun, H.; Gao, C. Coaxial Wet-Spun Yarn Supercapacitors for

DOI: 10.1021/acsami.8b19890
ACS Appl. Mater. Interfaces 2019, 11, 6541−6549

High-Energy Density and Safe Wearable Electronics. *Nat. Commun.* **2014**, *5*, 3754.
(19) Ma, W.; Liu, L.; Yang, R.; Zhang, T.; Zhang, Z.; Song, L.; Ren, Y.; Shen, J.; Niu, Z.; Zhou, W.; Xie, S. Monitoring a Micromechanical Process in Macroscale Carbon Nanotube Films and Fibers. *Adv. Mater.* **2008**, *21*, 603−608.
(20) Gao, Y.; Liu, L.-Q.; Zu, S.-Z.; Peng, K.; Zhou, D.; Han, B.-H.; Zhang, Z. The Effect of Interlayer Adhesion on the Mechanical Behaviors of Macroscopic Graphene Oxide Papers. *ACS Nano* **2011**, *5*, 2134−2141.
(21) Dai, Z.; Wang, Y.; Liu, L.; Liu, X.; Tan, P.; Xu, Z.; Kuang, J.; Liu, Q.; Lou, J.; Zhang, Z. Hierarchical Graphene-Based Films with Dynamic Self-Stiffening for Biomimetic Artificial Muscle. *Adv. Funct. Mater.* **2016**, *26*, 7003−7010.
(22) Kuang, J.; Liu, L.; Gao, Y.; Zhou, D.; Chen, Z.; Han, B.; Zhang, Z. A Hierarchically Structured Graphene Foam and Its Potential as a Large-Scale Strain-Gauge Sensor. *Nanoscale* **2013**, *5*, 12171−12177.
(23) Dai, Z.; Liu, L.; Qi, X.; Kuang, J.; Wei, Y.; Zhu, H.; Zhang, Z. Three-dimensional Sponges with Super Mechanical Stability: Harnessing True Elasticity of Individual Carbon Nanotubes in Macroscopic Architectures. *Sci. Rep.* **2016**, *6*, 18930.
(24) Qian, F.; Lan, P. C.; Freyman, M. C.; Chen, W.; Kou, T.; Olson, T. Y.; Zhu, C.; Worsley, M. A.; Duoss, E. B.; Spadaccini, C. M.; Baumann, T.; Han, T. Y.-J. Ultralight Conductive Silver Nanowire Aerogels. *Nano Lett.* **2017**, *17*, 7171−7176.
(25) Worsley, M. A.; Kucheyev, S. O.; Satcher, J. H.; Hamza, A. V.; Baumann, T. F. Mechanically Robust and Electrically Conductive Carbon Nanotube Foams. *Appl. Phys. Lett.* **2009**, *94*, 073115.
(26) Dai, Z.; Weng, C.; Liu, L.; Hou, Y.; Zhao, X.; Kuang, J.; Shi, J.; Wei, Y.; Lou, J.; Zhang, Z. Multifunctional Polymer-Based Graphene Foams with Buckled Structure and Negative Poisson's Ratio. *Sci. Rep.* **2016**, *6*, 32989.
(27) Cheng, Y.; Wang, R.; Sun, J.; Gao, L. A Stretchable and Highly Sensitive Graphene-Based Fiber for Sensing Tensile Strain, Bending, and Torsion. *Adv. Mater.* **2015**, *27*, 7365−7371.
(28) Zhang, Y.; Zhang, L.; Zhang, G.; Li, H. Naturally Dried Graphene-Based Nanocomposite Aerogels with Exceptional Elasticity and High Electrical Conductivity. *ACS Appl. Mater. Interfaces* **2018**, *10*, 21565−21572.
(29) Zhu, C.-H.; Li, L.-M.; Wang, J.-H.; Wu, Y.-P.; Liu, Y. Three-Dimensional Highly Conductive Silver Nanowires Sponges Based on Cotton-Templated Porous Structures for Stretchable Conductors. *RSC Adv.* **2017**, *7*, 51−57.
(30) Wang, R.; Zhai, H.; Wang, T.; Wang, X.; Cheng, Y.; Shi, L.; Sun, J. Plasma-Induced Nanowelding of a Copper Nanowire Network and Its Application in Transparent Electrodes and Stretchable Conductors. *Nano Res.* **2016**, *9*, 2138−2148.
(31) Huang, D.; Liao, F.; Molesa, S.; Redinger, D.; Subramanian, V. Plastic-Compatible Low Resistance Printable Gold Nanoparticle Conductors for Flexible Electronics. *J. Electrochem. Soc.* **2003**, *150*, G412−G417.
(32) Wang, G.; Dai, Z.; Wang, Y.; Tan, P.; Liu, L.; Xu, Z.; Wei, Y.; Huang, R.; Zhang, Z. Measuring Interlayer Shear Stress in Bilayer Graphene. *Phys. Rev. Lett.* **2017**, *119*, 036101.
(33) Shang, Y.; He, X.; Li, Y.; Zhang, L.; Li, Z.; Ji, C.; Shi, E.; Li, P.; Zhu, K.; Peng, Q.; Wang, C.; Zhang, X.; Wang, R.; Wei, J.; Wang, K.; Zhu, H.; Wu, D.; Cao, A. Super-Stretchable Spring-Like Carbon Nanotube Ropes. *Adv. Mater.* **2012**, *24*, 2896−2900.
(34) Blees, M. K.; Barnard, A. W.; Rose, P. A.; Roberts, S. P.; McGill, K. L.; Huang, P. Y.; Ruyack, A. R.; Kevek, J. W.; Kobrin, B.; Muller, D. A.; McEuen, P. L. Graphene kirigami. *Nature* **2015**, *524*, 204−207.
(35) Yang, S.; Chen, Y.-C.; Nicolini, L.; Pasupathy, P.; Sacks, J.; Su, B.; Yang, R.; Sanchez, D.; Chang, Y.-F.; Wang, P.; Schnyer, D.; Neikirk, D.; Lu, N. "Cut-and-Paste" Manufacture of Multiparametric Epidermal Sensor Systems. *Adv. Mater.* **2015**, *27*, 6423−6430.
(36) Xu, F.; Wang, X.; Zhu, Y.; Zhu, Y. Wavy Ribbons of Carbon Nanotubes for Stretchable Conductors. *Adv. Funct. Mater.* **2012**, *22*, 1279−1283.
(37) Lakes, R. Foam structures with a negative Poisson's ratio. *Science* **1987**, *235*, 1038−1040.
(38) Li, Y.; Luo, S.; Yang, M.-C.; Liang, R.; Zeng, C. Poisson Ratio and Piezoresistive Sensing: A New Route to High-Performance 3D Flexible and Stretchable Sensors of Multimodal Sensing Capability. *Adv. Funct. Mater.* **2016**, *26*, 2900−2908.
(39) Lee, H.; Dellatore, S. M.; Miller, W. M.; Messersmith, P. B. Mussel-Inspired Surface Chemistry for Multifunctional Coatings. *Science* **2007**, *318*, 426−430.
(40) Lee, H.; Lee, Y.; Statz, A. R.; Rho, J.; Park, T. G.; Messersmith, P. B. Substrate-Independent Layer-by-Layer Assembly by Using Mussel-Adhesive-Inspired Polymers. *Adv. Mater.* **2008**, *20*, 1619−1623.
(41) Kang, S. M.; Park, S.; Kim, D.; Park, S. Y.; Ruoff, R. S.; Lee, H. Simultaneous Reduction and Surface Functionalization of Graphene Oxide by Mussel-Inspired Chemistry. *Adv. Funct. Mater.* **2010**, *21*, 108−112.
(42) Akter, T.; Kim, W. S. Reversibly Stretchable Transparent Conductive Coatings of Spray-Deposited Silver Nanowires. *ACS Appl. Mater. Interfaces* **2012**, *4*, 1855−1859.
(43) Xie, Y.; Zheng, Y.; Fan, J.; Wang, Y.; Yue, L.; Zhang, N. Novel Electronic-Ionic Hybrid Conductive Composites for Multifunctional Flexible Bioelectrode Based on in Situ Synthesis of Poly(dopamine) on Bacterial Cellulose. *ACS Appl. Mater. Interfaces* **2018**, *10*, 22692−22702.
(44) Greaves, G. N.; Greer, A. L.; Lakes, R. S.; Rouxel, T. Poisson's Ratio and Modern Materials. *Nat. Mater.* **2011**, *10*, 823−837.
(45) Qiu, L.; Liu, J. Z.; Chang, S. L.; Wu, Y.; Li, D. Biomimetic Superelastic Graphene-Based Cellular Monoliths. *Nat. Commun.* **2012**, *3*, 1241.
(46) Zhang, X.; Sui, Z.; Xu, B.; Yue, S.; Luo, Y.; Zhan, W.; Liu, B. Mechanically Strong and Highly Conductive Graphene Aerogel and Its Use as Electrodes for Electrochemical Power Sources. *J. Mater. Chem.* **2011**, *21*, 6494−6497.
(47) Zou, J.; Liu, J.; Karakoti, A. S.; Kumar, A.; Joung, D.; Li, Q.; Khondaker, S. I.; Seal, S.; Zhai, L. Ultralight Multiwalled Carbon Nanotube Aerogel. *ACS Nano* **2010**, *4*, 7293−7302.
(48) Worsley, M. A.; Pauzauskie, P. J.; Olson, T. Y.; Biener, J.; Satcher, J. H.; Baumann, T. F. Synthesis of Graphene Aerogel with High Electrical Conductivity. *J. Am. Chem. Soc.* **2010**, *132*, 14067−14069.
(49) Worsley, M. A.; Olson, T. Y.; Lee, J. R. I.; Willey, T. M.; Nielsen, M. H.; Roberts, S. K.; Pauzauskie, P. J.; Biener, J.; Satcher, J. H., Jr.; Baumann, T. F. High Surface Area, sp2-Cross-Linked Three-Dimensional Graphene Monoliths. *J. Phys. Chem. Lett.* **2011**, *2*, 921−925.
(50) Gui, X.; Cao, A.; Wei, J.; Li, H.; Jia, Y.; Li, Z.; Fan, L.; Wang, K.; Zhu, H.; Wu, D. Soft, Highly Conductive Nanotube Sponges and Composites with Controlled Compressibility. *ACS Nano* **2010**, *4*, 2320−2326.
(51) Kim, K. H.; Oh, Y.; Islam, M. F. Graphene Coating Makes Carbon Nanotube Aerogels Superelastic and Resistant to Fatigue. *Nat. Nanotechnol.* **2012**, *7*, 562−566.
(52) Wang, Z.; Liu, X.; Shen, X.; Han, N. M.; Wu, Y.; Zheng, Q.; Jia, J.; Wang, N.; Kim, J.-K. An Ultralight Graphene Honeycomb Sandwich for Stretchable Light-Emitting Displays. *Adv. Funct. Mater.* **2018**, *28*, 1707043.
(53) Guo, F.; Jiang, Y.; Xu, Z.; Xiao, Y.; Fang, B.; Liu, Y.; Gao, W.; Zhao, P.; Wang, H.; Gao, C. Highly Stretchable Carbon Aerogels. *Nat. Commun.* **2018**, *9*, 881.
(54) Zhang, R.; Hu, R.; Li, X.; Zhen, Z.; Xu, Z.; Li, N.; He, L.; Zhu, H. A Bubble-Derived Strategy to Prepare Multiple Graphene-Based Porous Materials. *Adv. Funct. Mater.* **2018**, *28*, 1705879.
(55) Ge, J.; Yao, H.-B.; Wang, X.; Ye, Y.-D.; Wang, J.-L.; Wu, Z.-Y.; Liu, J.-W.; Fan, F.-J.; Gao, H.-L.; Zhang, C.-L.; Yu, S.-H. Stretchable Conductors Based on Silver Nanowires: Improved Performance Through a Binary Network Design. *Angew. Chem., Int. Ed.* **2013**, *52*, 1654−1659.

DOI: 10.1021/acsami.8b19890
ACS Appl. Mater. Interfaces 2019, 11, 6541−6549

(56) Gao, H.-L.; Xu, L.; Long, F.; Pan, Z.; Du, Y.-X.; Lu, Y.; Ge, J.; Yu, S.-H. Macroscopic Free-Standing Hierarchical 3D Architectures Assembled from Silver Nanowires by Ice Templating. *Angew. Chem., Int. Ed.* **2014**, *53*, 4561−4566.
(57) Liang, H.-W.; Guan, Q.-F.; Zhu, Z.; Song, L.-T.; Yao, H.-B.; Lei, X.; Yu, S.-H. Highly Conductive and Stretchable Conductors Fabricated from Bacterial Cellulose. *NPG Asia Mater.* **2012**, *4*, No. e19.
(58) Kim, K. H.; Vural, M.; Islam, M. F. Single-Walled Carbon Nanotube Aerogel-Based Elastic Conductors. *Adv. Mater.* **2011**, *23*, 2865−2869.
(59) Shin, M. K.; Oh, J.; Lima, M.; Kozlov, M. E.; Kim, S. J.; Baughman, R. H. Elastomeric Conductive Composites Based on Carbon Nanotube Forests. *Adv. Mater.* **2010**, *22*, 2663−2667.
(60) Chen, Z.; Ren, W.; Gao, L.; Liu, B.; Pei, S.; Cheng, H.-M. Three-Dimensional Flexible and Conductive Interconnected Graphene Networks Grown by Chemical Vapour Deposition. *Nat. Mater.* **2011**, *10*, 424−428.
(61) Duan, S.; Wang, Z.; Zhang, L.; Liu, J.; Li, C. Three-Dimensional Highly Stretchable Conductors from Elastic Fiber Mat with Conductive Polymer Coating. *ACS Appl. Mater. Interfaces* **2017**, *9*, 30772−30778.
(62) Han, F.; Su, X.; Huang, M.; Li, J.; Zhang, Y.; Zhao, S.; Liu, F.; Zhang, B.; Wang, Y.; Zhang, G.; Sun, R.; Wong, C.-P. Fabrication of a flexible and stretchable three-dimensional conductor based on Au-Ni@graphene coated polyurethane sponge by electroless plating. *J. Mater. Chem. C* **2018**, *6*, 8135−8143.
(63) Hong, S.; Lee, H.; Lee, J.; Kwon, J.; Han, S.; Suh, Y. D.; Cho, H.; Shin, J.; Yeo, J.; Ko, S. H. Highly Stretchable and Transparent Metal Nanowire Heater for Wearable Electronics Applications. *Adv. Mater.* **2015**, *27*, 4744−4751.
(64) An, B. W.; Gwak, E.-J.; Kim, K.; Kim, Y.-C.; Jang, J.; Kim, J.-Y.; Park, J.-U. Stretchable, Transparent Electrodes as Wearable Heaters Using Nanotrough Networks of Metallic Glasses with Superior Mechanical Properties and Thermal Stability. *Nano Lett.* **2015**, *16*, 471−478.
(65) Wang, R.; Xu, Z.; Zhuang, J.; Liu, Z.; Peng, L.; Li, Z.; Liu, Y.; Gao, W.; Gao, C. Highly Stretchable Graphene Fibers with Ultrafast Electrothermal Response for Low-Voltage Wearable Heaters. *Adv. Electron. Mater.* **2016**, *3*, 1600425.
(66) Lee, J.; Lee, P.; Lee, H.; Lee, D.; Lee, S. S.; Ko, S. H. Very Long Ag Nanowire Synthesis and Its Application in a Highly Transparent, Conductive and Flexible Metal Electrode Touch Panel. *Nanoscale* **2012**, *4*, 6408−6414.
(67) Jiu, J.; Araki, T.; Wang, J.; Nogi, M.; Sugahara, T.; Nagao, S.; Koga, H.; Suganuma, K.; Nakazawa, E.; Hara, M.; Uchida, H.; Shinozaki, K. Facile Synthesis of Very-Long Silver Nanowires for Transparent Electrodes. *J. Mater. Chem. A* **2014**, *2*, 6326−6330.

DOI: 10.1021/acsami.8b19890
ACS Appl. Mater. Interfaces 2019, 11, 6541−6549